



3D interconnected Bi₂S₃ nanosheets network directly grown on nickel foam as advanced performance binder-free electrode for hybrid asymmetric supercapacitor

Xiangang Zhai^{a,b}, Jianping Gao^{a,**}, Xiaoyang Xu^c, Wei Hong^a, Huan Wang^a, Fuming Wu^a, Yu Liu^{a,*}

^a Department of Chemistry, School of Science, Tianjin University, Tianjin, 300072, PR China

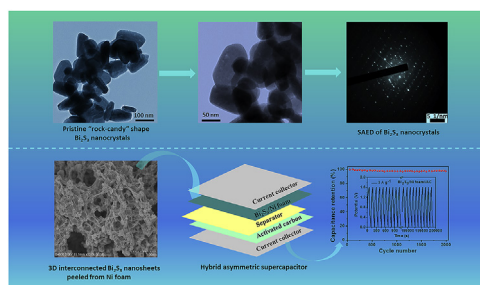
^b Key Laboratory of Sichuan Province for Metal Fuel Cell, DeYang, 618029, Sichuan, PR China

^c School of Chemical and Pharmaceutical Engineering, Hebei University of Science and Technology, PR China

HIGHLIGHTS

- Ammonium bismuth citrate (C₁₂H₂₂BiN₃O₁₄) was used as a novel bismuth source.
- “rock-candy” shape Bi₂S₃ nanocrystals were successfully synthesized.
- The 3D interconnected Bi₂S₃/Ni foam was directly used as working electrode.
- The specific capacity of Bi₂S₃/Ni foam can reach 500.8 mAh g^{−1} at 0.5 A g^{−1}.
- The hybrid asymmetric device exhibited excellent supercapacitive performances.

GRAPHICAL ABSTRACT



ARTICLE INFO

Keywords:

Hybrid asymmetric supercapacitor
3D interconnected Bi₂S₃ nanosheets network
Activated carbon
Hydrothermal approach
“rock-candy” shape Bi₂S₃ nanocrystals

ABSTRACT

In this paper, we report the successful synthesis of “rock-candy” shape Bi₂S₃ nanocrystals and 3D interconnected Bi₂S₃ nanosheets network on Ni foam by a facile hydrothermal method. The structure and composition of the as-synthesized products were characterized by XRD, XPS, SEM and TEM analyses. The unique structure makes them have high electrochemical properties. At current density of 0.5 A g^{−1}, the binder-free Bi₂S₃/Ni foam working electrode with high specific area possesses high specific capacity (500.8 mAh g^{−1}) compared to pristine Bi₂S₃ (245.5 mAh g^{−1}). In the actual application of Bi₂S₃/Ni foam, the assembled Bi₂S₃/Ni foam//AC hybrid asymmetric supercapacitor exhibits excellent supercapacitive performances, such as high specific capacitance (148.7 F g^{−1} at 1 A g^{−1}), high energy density (45.1 Wh Kg^{−1} at 3202 W Kg^{−1}), excellent cycling stability (capacitance retention is about 98.7% after 2000 cycles at a current density of 3 A g^{−1}) and low Warburg and charge transfer resistances.

1. Introduction

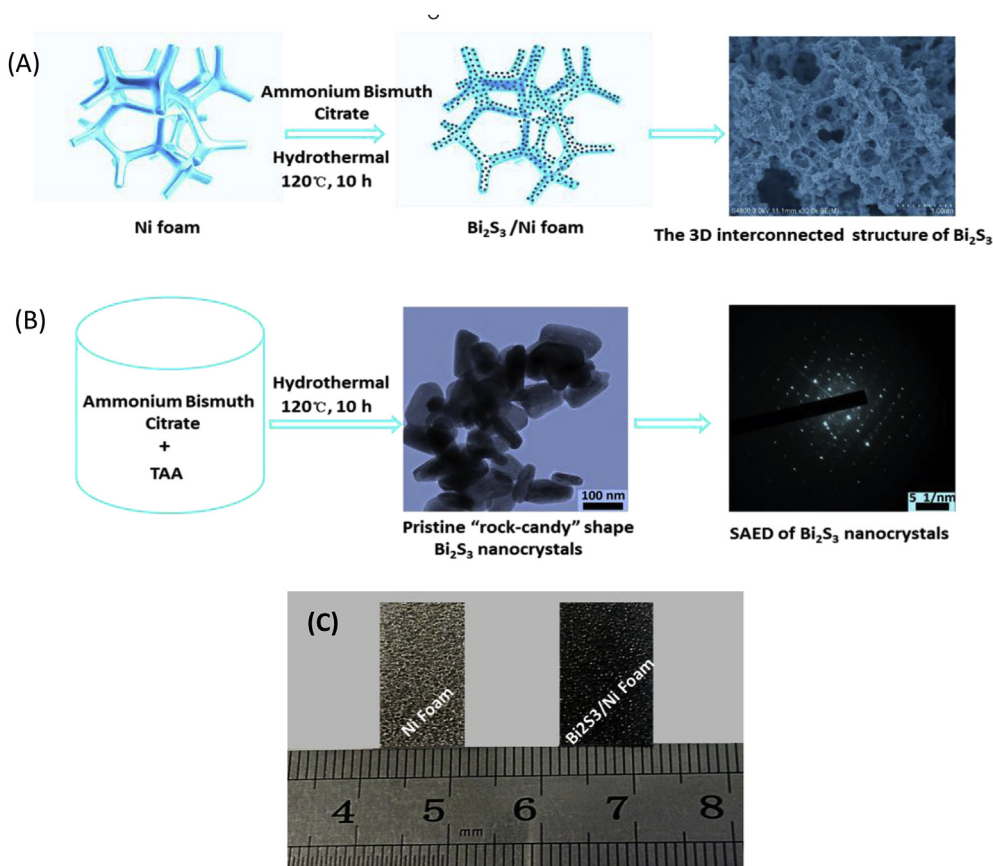
Facing a severe global energy crisis and environmental pollution, as

well as the ever-growing needs for green energy conversion devices, portable electronic devices and hybrid electric vehicles, considerable efforts have been made in exploring advanced performance and eco-

* Corresponding author.

** Corresponding author.

E-mail address: tjly@tju.edu.cn (Y. Liu).



Scheme 1. Schematic illustration of the preparation of Bi₂S₃/Ni foam (A) and pristine Bi₂S₃ (B). Digital photographs of Ni foam before and after growth of Bi₂S₃ (C).

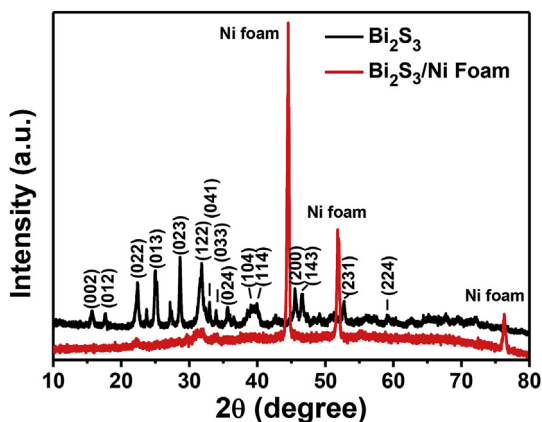


Fig. 1. XRD patterns of pristine Bi₂S₃ and Bi₂S₃/Ni foam.

friendly energy storage devices in the past several decades [1–5]. Electrochemical capacitors, which are also called supercapacitors (SCs), have attracted tremendous interest owing to their outstanding merits, such as high energy and power densities, fast discharge/charge process and long cycle life [6–8].

In general, according to the different charge storage mechanisms, supercapacitors can be categorized into two types, the electrochemical double layer capacitors (EDLCs) and pseudocapacitors (redox supercapacitors) [9,10]. EDLCs based on the reversible ion-absorption at the electrolyte/electrode interface using carbon materials have been widely used because of their low-cost, excellent electrical conductivity and high cycle stability [7,11–14]. However, the low capacity of these carbon-based electrode materials hinders their commercial applications. Pseudocapacitors, which are based on the reversible Faradic

redox reactions at the surface of electrode materials via using conducting polymers such as polypyrrole (PPy) and polyaniline (PANI). In recent years, transition metal chalcogenides (TMCs), have been considered as promising candidates for SCs [5,15–20]. Wherein, TMCs possess remarkable advantages such as higher theoretical capacities, better cycling stability compared with conducting polymers [6]. Therefore, the rational design and fabrication of high-performance TMCs electrode materials for SCs is still significant and necessary.

Up to now, considerable researches have been reported on the preparation of various kinds of TMCs for high-performance electrode materials for supercapacitor, such as CuS [17], Ni₃S₂ [18], MnS [21], CoS [22], Co_{1.5}Ni_{1.5}S₄ [23], SnS₂ [24] and MoS₂ [25]. However, few studies on the synthesis of bismuth sulfide (Bi₂S₃) for SCs materials have been investigated. Bi₂S₃, a laminar structured semiconductor with a direct band gap of 1.3 eV, has been widely applied in catalysis, thermoelectric devices, lithium-ion batteries and solar cells on account of its environmental benignity and excellent magnetic, optical, electrochemical and catalytic properties [26–30]. Unfortunately, similar to the transition metal oxides, the poor intrinsic conductivity of the Bi₂S₃ seriously hinders its electrochemical performance and further applications. To overcome the drawback, one effective method is to combine Bi₂S₃ with carbon matrix. Nie et al. synthesized Bi₂S₃ nanorods/reduced graphene oxide (rGO) composites via a facile one-pot hydrothermal approach and found that the composites exhibited enhanced electrochemical performance compared with the pristine rGO and Bi₂S₃ [6]. As we all know, the addition of conducting agent and polymer binder in the preparation of electrode will lead to low utilization of active materials and poor electron conductivity and may significantly limit the electrochemical performance of the electrodes [3,8]. Therefore, another feasible strategy is focused on the direct growth of electrode materials on the conductive substrates such as Ni foam and carbon cloth [7]. Such a binder-free method can not only enhance the

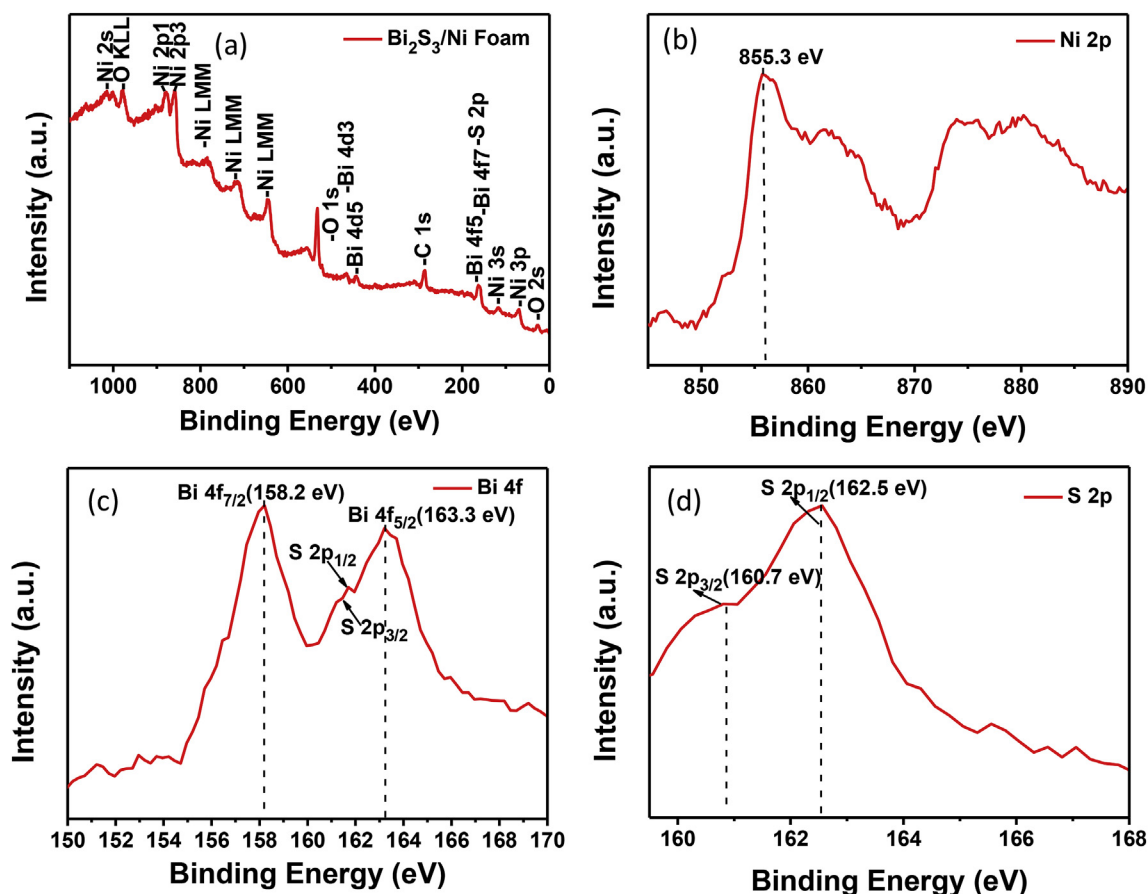


Fig. 2. XPS full spectrum of the as-synthesized $\text{Bi}_2\text{S}_3/\text{Ni}$ foam (a). Ni 2p (b), Bi 4f (c) and S 2p (d) high-resolution core level spectra of the $\text{Bi}_2\text{S}_3/\text{Ni}$ foam.

conductivity and the supercapacitive performance of the active materials, but can also vastly improve the adhesion of active materials to the current collector as well as the contact area of the interface between them [2,3]. Recently, various kinds of TMCs supercapacitors electrode materials grown on Ni foam have been investigated, such as interconnected CuS nanowalls [31], 3D CoS nanosheets [32], MoS_2 [33], monocrystalline NiS nanowire [34], MnS nanoclusters [35] and hybrid NiS/CoO mesoporous nanosheet [36]. However, few works have focused on Bi_2S_3 as supercapacitive electrode materials. To the best of our knowledge, fabrication of 3D interconnected Bi_2S_3 nanosheets network grown on Ni foam ($\text{Bi}_2\text{S}_3/\text{Ni}$ foam) for hybrid asymmetric supercapacitor has never been reported.

In this work, 3D interconnected Bi_2S_3 nanosheets network as high performance binder-free electrode was directly grown on Ni foam using a facile hydrothermal approach, and its application in hybrid asymmetric supercapacitor was investigated in detail for the first time. Specially, compared with “rock-candy” shape Bi_2S_3 nanocrystals (pristine Bi_2S_3) prepared under the same conditions and the reported similar works [6,9], 3D interconnected Bi_2S_3 nanosheets network exhibits obvious advantages as follows: (a) the interconnected Bi_2S_3 nanosheets grown on Ni foam can provide excellent electron conductivity via forming a 3D conductive network and greatly shorten the charge ions transport distance to the inner part of the electrode; (b) it can be directly employed as electrode without introduction of conducting agent and polymer binder, avoiding the inadequate contact between active materials and electrolyte because of the utilization of binder; (c) its unique structure can not only offer higher interfacial areas between the Ni foam and the active materials, but can also dramatically enhance electrochemical performances such as specific capacity and cycling stability due to its richness in accessible chemical reaction sites. In addition, in order to explore the practical application of the as-

synthesized $\text{Bi}_2\text{S}_3/\text{Ni}$ foam, the hybrid asymmetric supercapacitor ($\text{Bi}_2\text{S}_3/\text{Ni}$ foam//AC (activated carbon)) was assembled with $\text{Bi}_2\text{S}_3/\text{Ni}$ foam as the positive material and AC as the negative material. The 1 M KOH was employed as the electrolyte due to its low-cost, safety and environmental benignity [8]. Thus designed hybrid device can combine the advantages of the high capacity of $\text{Bi}_2\text{S}_3/\text{Ni}$ foam and the excellent cycling stability of AC. As expected, the hybrid asymmetric supercapacitor exhibited excellent supercapacitive performance and excellent cycling stability. In addition, the electrochemical tests demonstrated that the $\text{Bi}_2\text{S}_3/\text{Ni}$ foam electrode possessed higher specific capacity than the pristine Bi_2S_3 .

2. Experimental

2.1. Materials

All the chemical reagents in this work were used as received. Ammonium bismuth citrate ($\text{C}_{12}\text{H}_{22}\text{BiN}_3\text{O}_{14}$, ABC) and thioacetamide (TAA, $\text{C}_2\text{H}_5\text{NS}$) were obtained from Tianjin Yuanli Chemical Technology Company. Activated carbon was acquired from Qingdao Graphite Factory. Nickel foam was from Kunshan Dessco Electronics Company.

2.2. Preparation of $\text{Bi}_2\text{S}_3/\text{Ni}$ foam and pristine Bi_2S_3

The Ni foam was cut into small square pieces ($1.0 \times 2.5 \times 0.15 \text{ cm}^3$, 30 mg cm^{-2}) and then pretreated with acetone, ethanol and distilled water under ultrasound conditions to remove the surface oxide layer. In a typical procedure, 2 mmol of ABC and 3 mmol TAA were added into 70 mL distilled water under constant magnetic stirring to obtain a mixed solution. Subsequently, the mixed solution

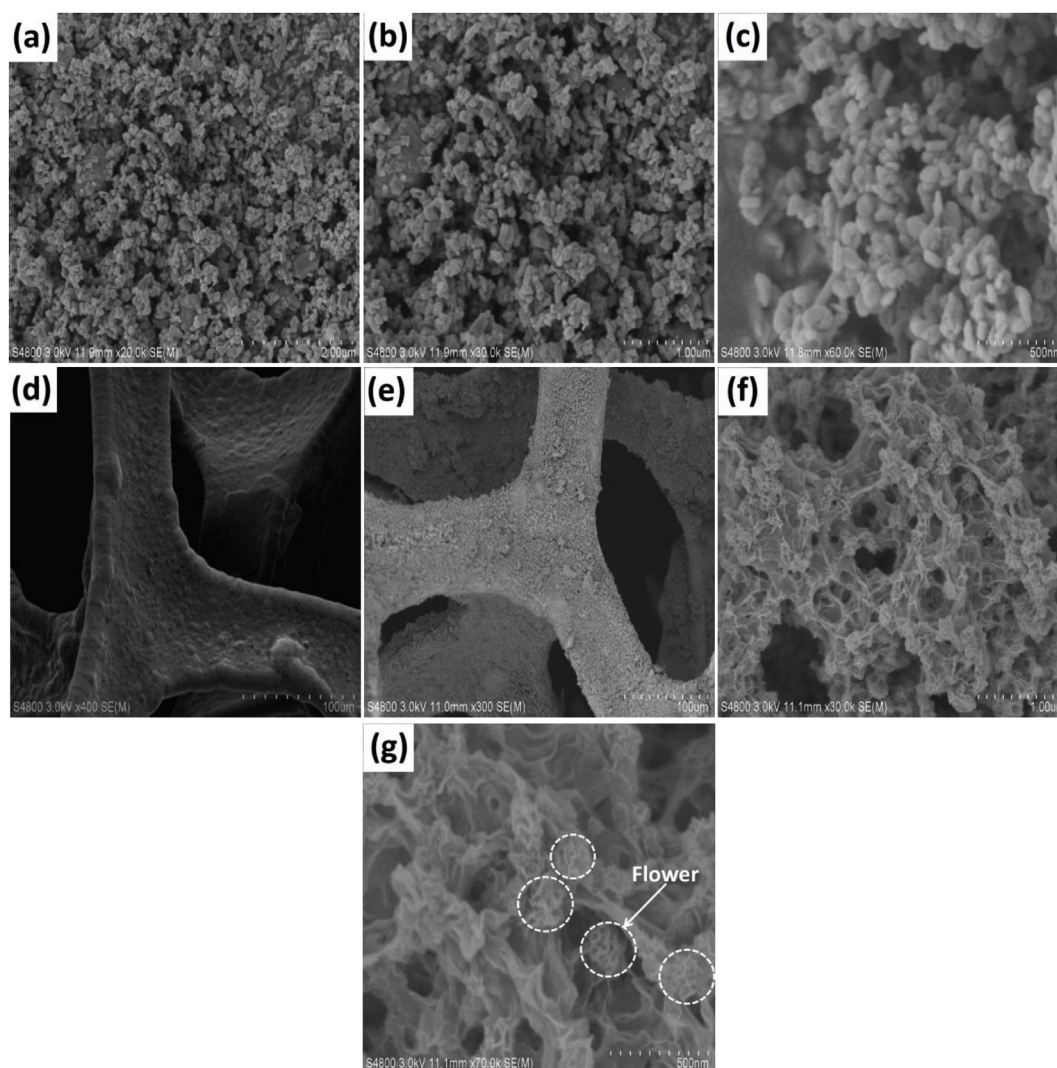


Fig. 3. SEM images of the pristine Bi₂S₃ (a–c), pristine Ni foam (d) and Bi₂S₃/Ni foam (e–g).

and the cleaned Ni foam were transferred into a 100 mL Teflon-lined stainless autoclave and maintained at 120 °C for 10 h in an oven. After cooling to room temperature, the coated Ni foam was washed with distilled water and absolute ethanol for several times, and then dried at 40 °C for 12 h in a vacuum oven to obtain the Bi₂S₃/Ni foam, which will be utilized as the working electrode directly. The pristine Bi₂S₃ was prepared under the same hydrothermal conditions.

2.3. Materials characterization

The morphologies of the as-prepared Bi₂S₃/Ni foam and the pristine Bi₂S₃ were observed using a transmission electron microscope (TEM, Philips Tecnai G2F20) at an acceleration voltage of 200 kV and a field-emission scanning electron microscope (SEM, FEI Nano SEM 430) at an acceleration voltage of 5 kV. The crystalline structures of the above products were characterized by an X-ray diffractometer (XRD, BRUKER AXS GMBH D8-Focus) with a Cu K α radiation ($\lambda = 1.54 \text{ \AA}$), voltage: 30 kV and current: 30 mA. The analysis of the surface elements of Bi₂S₃/Ni foam was conducted by an X-ray photoelectron spectrometer (XPS, PHI1600 ESCA System, PERKIN ELMER, US) with an Mg K α anode.

2.4. Electrochemical measurements

The Bi₂S₃/Ni foam ($1.0 \times 1.0 \text{ cm}^2$) was directly used as the working

electrode. As for the pristine Bi₂S₃ or AC, the working electrode was prepared as follows: the homogeneous paste of a sample, acetylene black and polytetrafluoroethylene binder (PTFE) with a mass ratio of 75:15:10 was coated and pressed onto the cleaned Ni foam ($1.0 \times 1.0 \text{ cm}^2$). The as-prepared electrodes were dried at 40 °C for 24 h in a vacuum oven. The electrochemical measurements including cyclic voltammetry (CV), galvanostatic charge-discharge (GCD) cycles and electrochemical impedance spectroscopy (EIS) of the as-prepared Bi₂S₃/Ni foam, pristine Bi₂S₃ and AC were conducted on a computer controlled workstation (CHI 660D) using a three-electrode system at room temperature. In the three-electrode system, a piece of Pt foil and HgO/Hg were used as the counter and reference electrodes, and 1 M KOH was used as the electrolyte.

The hybrid asymmetric supercapacitor was assembled with Bi₂S₃/Ni foam ($1.0 \times 1.0 \text{ cm}^2$) and AC as positive and negative electrodes. The cellulose membrane was used as separator and 1 M KOH was used as the electrolyte. Before assembling the hybrid device, the two working electrodes and the separator were soaked into 1 M KOH for 3 h. The electrochemical performance of the Bi₂S₃/Ni foam//AC hybrid asymmetric supercapacitor was investigated using a two-electrode system.

In the process of EIS tests, the frequency range was from 1×10^5 to $1 \times 10^{-2} \text{ Hz}$ with the applied potential amplitude of 5 mV at open circuit potential. The specific capacity of pristine Bi₂S₃ and Bi₂S₃/Ni foam electrode (Q , mAh g⁻¹), the specific capacitance of AC (C_s , F g⁻¹) and the hybrid asymmetric supercapacitor ($C_s(\text{has})$, F g⁻¹), the power

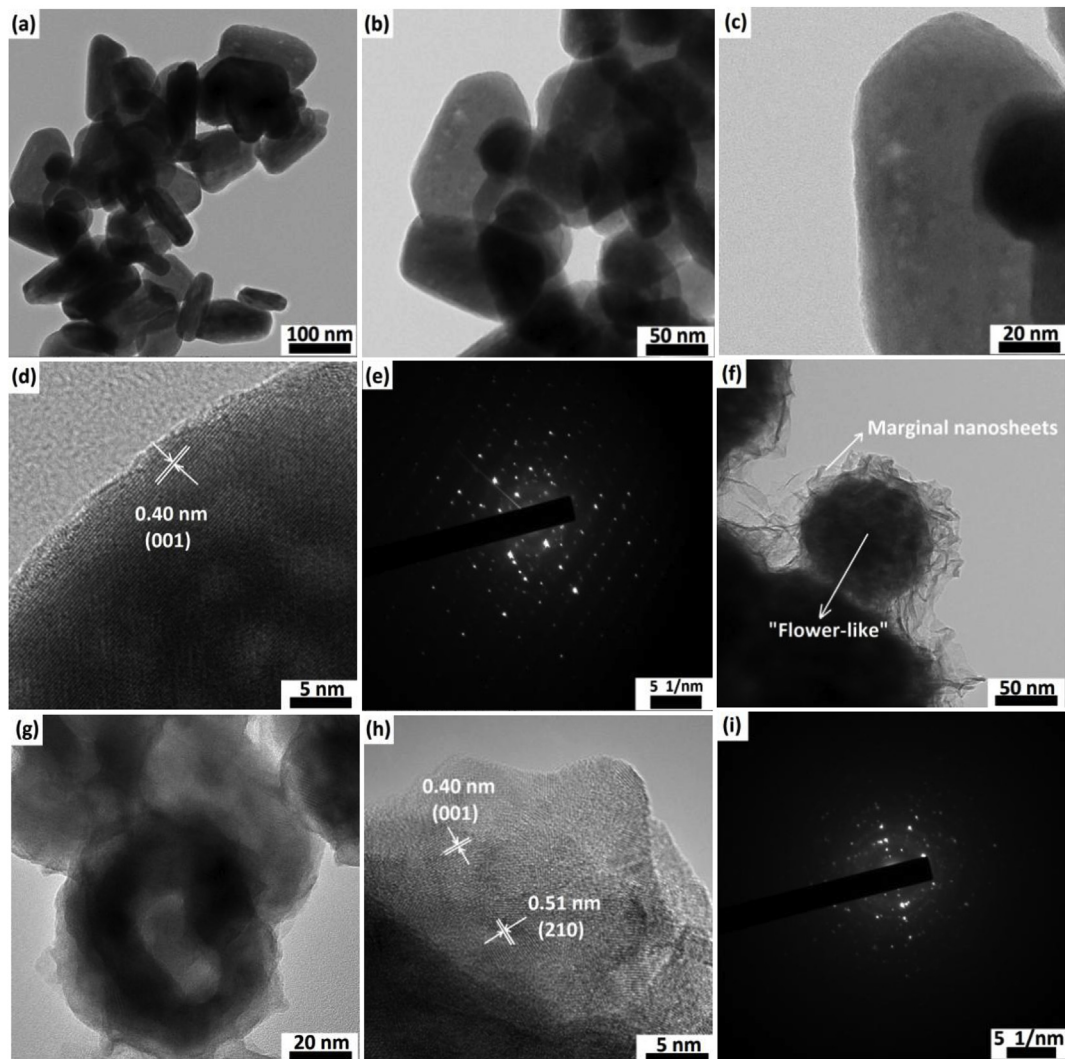


Fig. 4. TEM (a–c), HRTEM image (d) and SAED pattern (e) of the pristine Bi₂S₃. TEM (f–g), HRTEM image (h), SAED pattern (i) and EDS spectrum (j) of the 3D interconnected Bi₂S₃ nanosheets peeled from Ni foam.

density (P , W Kg^{−1}) and the energy density (E , Wh Kg^{−1}) of the hybrid asymmetric supercapacitor were calculated according to the following Eqs. (1)–(6) [4,37–39]:

$$Q = \frac{I \times t_d}{m} \quad (1)$$

$$Q = Cs \times \Delta v$$

$$Cs = \frac{I \times t_d}{m \times \Delta v} \quad (3)$$

$$Cs(has) = \frac{I \times t_d}{m \times \Delta v} \quad (4)$$

$$E = \frac{1000}{2 \times 3600} Cs(has)(\Delta v)^2 \quad (5)$$

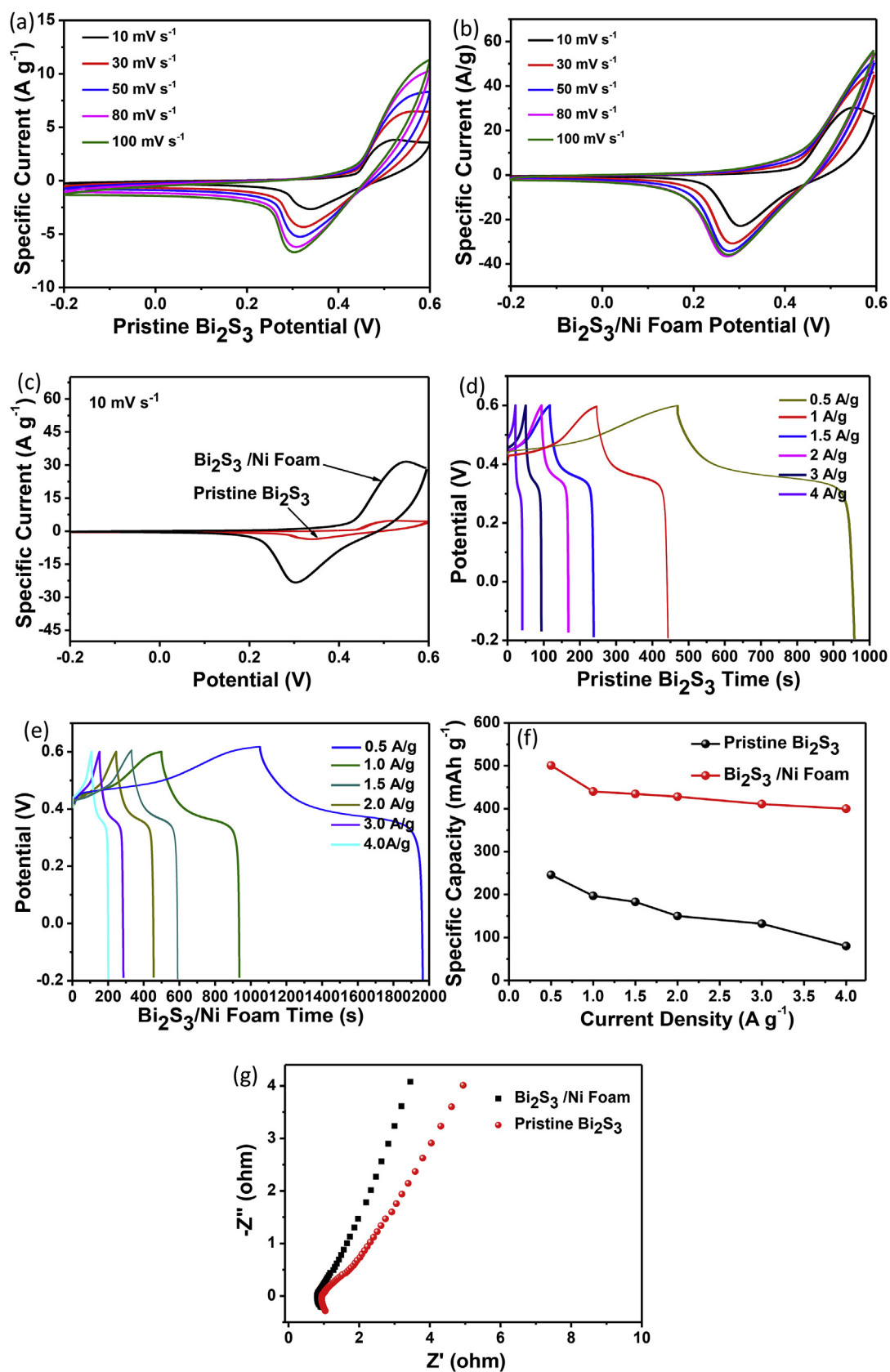


Fig. 5. CV curves at different scan rate (a–b); GCD curves at various current densities (d–e); specific capacities (f); Nyquist plots (g) for the pristine Bi_2S_3 and $\text{Bi}_2\text{S}_3/\text{Ni}$ foam in the three-electrode system. CV curves for the pristine Bi_2S_3 and $\text{Bi}_2\text{S}_3/\text{Ni}$ foam at a scan rate of 10 mV s^{-1} (c).

Table 1
Capacity comparison of several reported electrodes for supercapacitor.

Electrode	Current ($A\ g^{-1}$)	Q ($mAh\ g^{-1}$)	Electrolyte	Reference
Bi ₂ S ₃ /Ni foam	1 $A\ g^{-1}$	440	1 M KOH	Our work
BGNS-1	1 $A\ g^{-1}$	237	2 M KOH	[6]
Bi ₂ S ₃ /PbS	1 $mA\ cm^{-2}$	322	0.5 M Na ₂ SO ₄	[45]
Bi ₂ S ₃ /FGS	1 $A\ g^{-1}$	263	1 M Na ₂ SO ₄	[48]
WS ₂ /rGO	0.5 $A\ g^{-1}$	350	1 M Na ₂ SO ₄	[49]
Co-S-80	1 $A\ g^{-1}$	147	6 M KOH	[50]
BG composite	1 $A\ g^{-1}$	348	2 M KOH	[51]
MoS ₂ /Mn ₃ O ₄	1 $A\ g^{-1}$	50	1 M Na ₂ SO ₄	[52]

Cs: specific capacity; BGNS: Bi₂S₃ nanorods-rGO nanosheet composites; FGS: functionalized graphene nanosheets; BG: Bi₂S₃ nanorods-graphene.

$$P = \frac{3600 \times E}{\Delta t} \quad (6)$$

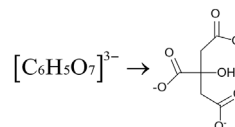
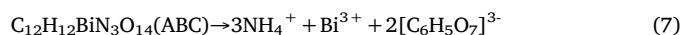
Where I is the given current (A), t_d is discharge time (s), Δv is the potential window (V), m and M refer to the mass (g) of active materials in the single electrode and in the Bi₂S₃-AC electrodes of hybrid asymmetric supercapacitor, respectively.

3. Results and discussion

3.1. Characterization of Bi₂S₃/Ni foam and pristine Bi₂S₃

The fabrication process of Bi₂S₃/Ni foam and the pristine Bi₂S₃ is schematically illustrated in Scheme 1. For the preparation of Bi₂S₃/Ni foam (Scheme 1A), a small square piece of pretreated Ni foam was immersed into a mixed solution containing 2 mmol ABC and 3 mmol TAA. Next, in the hydrothermal process, Bi₂S₃ nanosheets, which derived from the precipitation of Bi³⁺ and S²⁻, assembled on the Ni foam

and formed 3D interconnected network. The corresponding digital photos of pure Ni foam and Bi₂S₃/Ni foam are shown in Scheme 1C. Obviously, the color of the Ni foam changed to black, indicating the successful growth of Bi₂S₃ on the Ni foam. The mass loading of Bi₂S₃ per area on the Ni foam is calculated to be 3 mg cm⁻². Scheme 1B shows the preparation of pristine Bi₂S₃. The TEM image and the corresponding selected area electron diffraction (SAED) pattern demonstrate that the single-crystalline characteristic of the “rock-candy” shape pristine Bi₂S₃. The possible overall chemical reactions that occurred during the formation of Bi₂S₃ could be proposed in the following Eqs. (7)–(9):



To validate the crystal structures and phase purities of the as-prepared Bi₂S₃/Ni foam and pristine Bi₂S₃, the XRD patterns were measured. The XRD patterns of the Bi₂S₃/Ni foam and pristine Bi₂S₃ are shown in Fig. 1. It can be seen from the curve of the pristine Bi₂S₃ that the characteristic peaks at 15.6°, 17.6°, 22.4°, 24.9°, 28.6°, 31.8°, 33.1°, 33.9°, 35.6°, 39.1°, 39.9°, 45.5°, 46.5°, 52.7° and 59.1° can be assigned to (002), (012), (022), (013), (023), (122), (041), (033), (024), (104), (114), (200), (143), (231) and (224) planes, respectively. The XRD pattern demonstrates that the phase structure of the pristine Bi₂S₃ is orthorhombic in the Pmcn₆₂ space group (JCPDF No. 84-0279). The XRD pattern of Bi₂S₃/Ni foam is similar to that of the pristine Bi₂S₃.

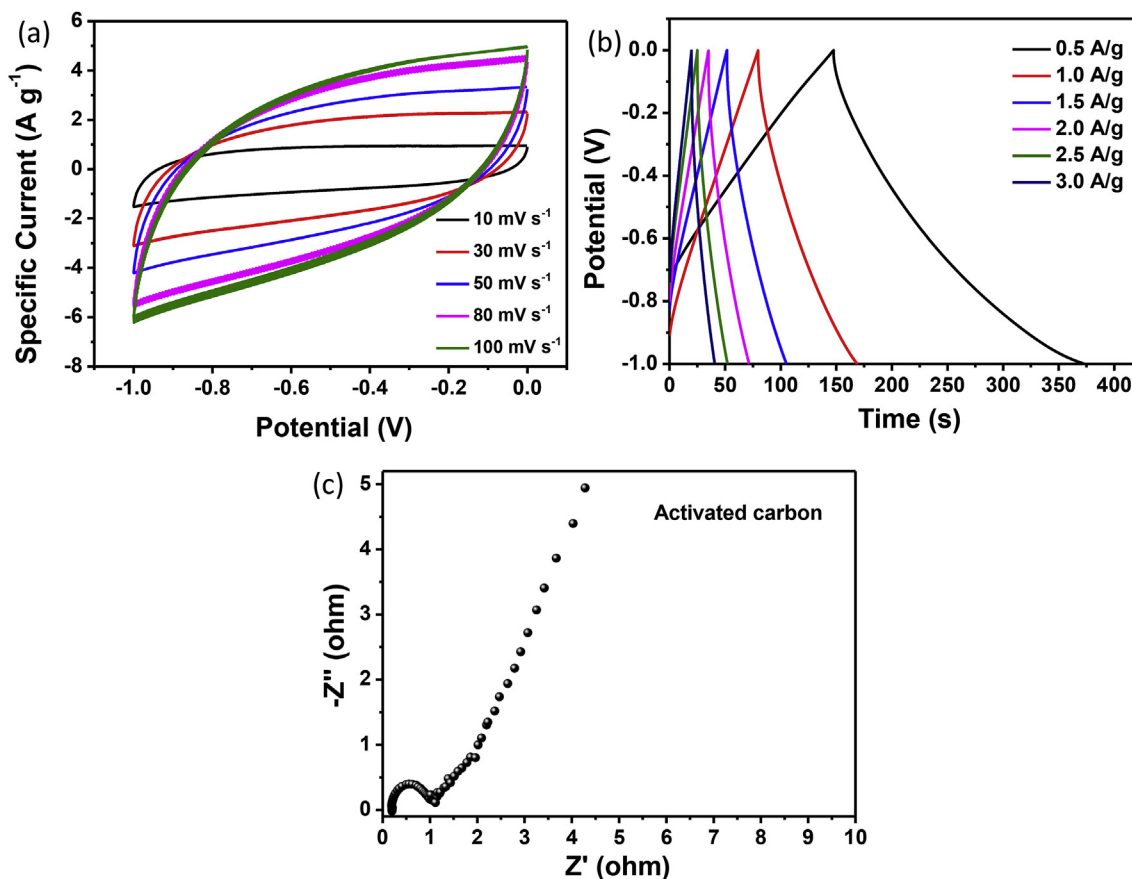


Fig. 6. CV curves at different scan rate (a), GCD curves at various current densities (b) and Nyquist plots (c) for AC in a three-electrode setup.

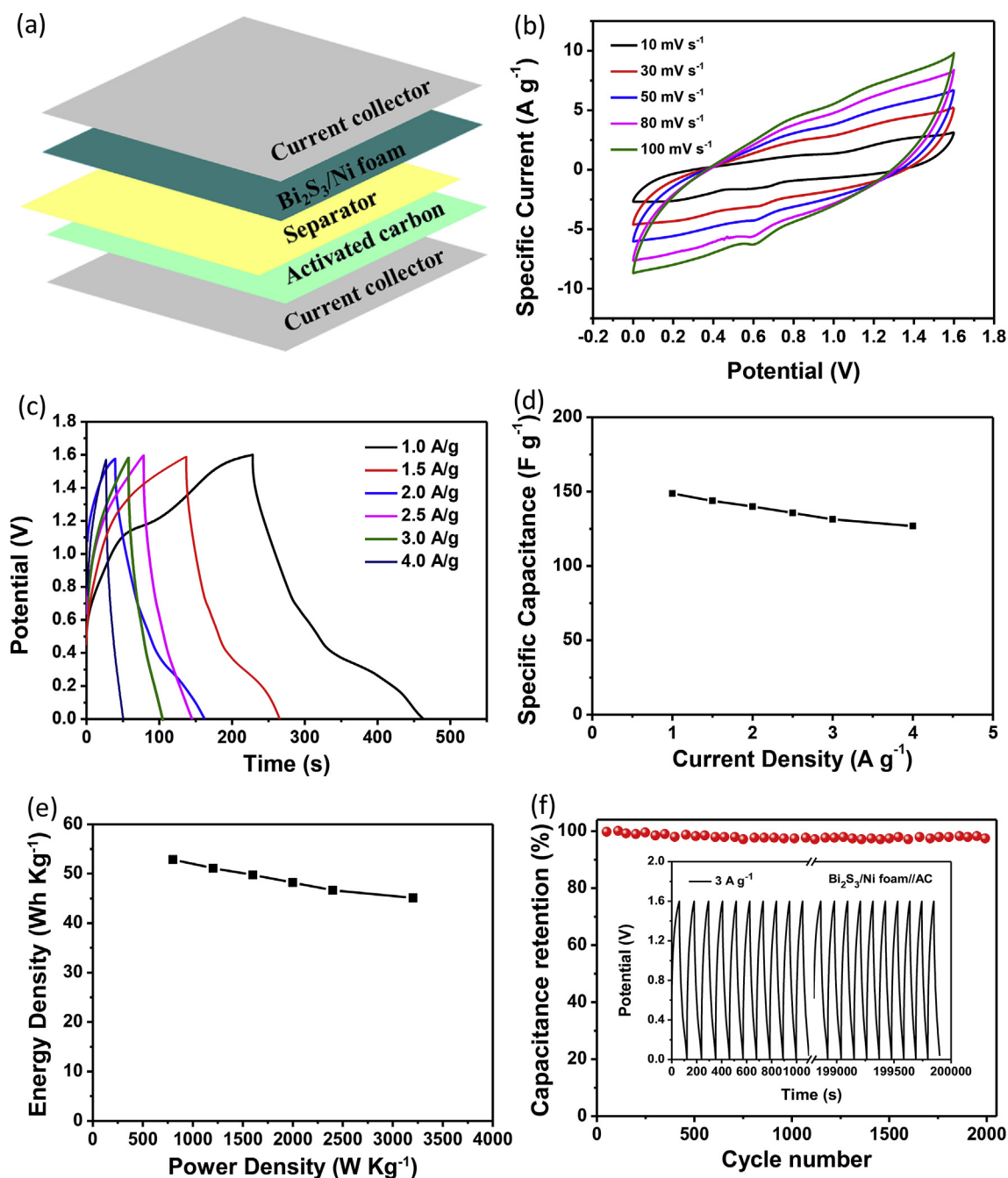


Fig. 7. The schematic illustration of the $\text{Bi}_2\text{S}_3/\text{Ni}$ foam//AC hybrid asymmetric supercapacitor (a); CV curves at different scan rates (b); GCD curves at various current densities based on the total mass of the active materials (c); specific capacitance (d), Ragone plot (e), capacitance retention after 2000 cycles at 3 A g^{-1} (f) and Nyquist plot (g) for the hybrid asymmetric supercapacitor.

Table 2

Energy density and power density of several reported electrodes for supercapacitor.

Electrode	E (Wh Kg^{-1})	P (W Kg^{-1})	Reference
$\text{Bi}_2\text{S}_3/\text{Ni}$ foam	45.1	3202.8	Our work
$\text{Bi}_2\text{S}_3/\text{PbS}$	20.1	1200	[45]
Co-S-80	14.25	150	[48]
CoS	14.25	1500	[50]
CuS	6.23	1750	[54]

E : energy density; P : power density.

Additionally, there are three strong peaks at $2\theta = 44.7^\circ$, 51.9° and 76.5° , which are derived from the Ni foam.

In order to further analyze the surface chemical composition and oxidation state of the $\text{Bi}_2\text{S}_3/\text{Ni}$ foam, XPS was performed and the results are shown in Fig. 2. The XPS survey spectrum (Fig. 2a–d) explicitly reveals the existence of Bi and S elements (C and O signals may derive from ambient impurities such as CO_2 and H_2O , Ni peaks come from the Ni foam). In Fig. 2b, the Ni 2p high-resolution spectrum possesses a main peak at about 855.3 eV, indicating that Ni exists in a bivalent form [40]. The high-resolution XPS spectra of Bi 4f and S 2p are shown in Fig. 2c–d. As shown in Fig. 2c, the binding energies located at 163.3 and 158.2 eV can be attributed to Bi^{3+} peaks of Bi_2S_3 . Moreover, the two peaks in Fig. 2c between Bi $4f_{5/2}$ and Bi $4f_{7/2}$ can be ascribed to S $2p_{1/2}$

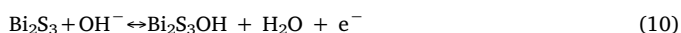
(162.5 eV) and S 2p_{3/2} (160.7 eV) shown in Fig. 2d [6,25,41–43].

The morphology and microstructure of the pristine Bi₂S₃ and Bi₂S₃/Ni foam were characterized by SEM, TEM and high-resolution TEM (HRTEM). Fig. 3a–c show the SEM images of the pristine Bi₂S₃ nanocrystals with “rock-candy” shape at different magnifications. Fig. 3d shows the SEM image of the pristine Ni foam with smooth surface. After hydrothermal reduction, a huge 3D interconnected Bi₂S₃ nanosheets network supported by the Ni foam is observed (Fig. 3e–g). Surprisingly, some “flower-like” spheres exist in the network (Fig. 3g), which is in good accordance with the TEM images (Fig. 4f–g). Fig. 4a–d shows the TEM images of the pristine Bi₂S₃ at different magnifications. There are many homogeneous “rock-candy” shape Bi₂S₃ nanocrystals with size of 50–150 nm and thickness of 20–50 nm (Fig. 4a–c). The spacing between two adjacent lattice fringes of the pristine Bi₂S₃ nanocrystals (Fig. 4d) is 0.40 nm, which is in good accordance of the standard interlayer distance of orthorhombic Bi₂S₃ (001) plane [44]. The SAED pattern in Fig. 4e indicates the single-crystalline characteristic of the pristine orthorhombic Bi₂S₃. Fig. 4f shows the TEM image of Bi₂S₃ peeled from Ni foam. There are some “flower-like” Bi₂S₃ spheres, which are composed of Bi₂S₃ nanosheets (Fig. 4g). HRTEM image of 3D interconnected Bi₂S₃ nanosheets in Fig. 4h shows the (001) and (210) lattice fringes with spacing of 0.40 and 0.51 nm. The SAED pattern in Fig. 4i displays diffraction rings of the 3D interconnected Bi₂S₃ nanosheets, demonstrating the poly-crystalline nature of the sample. In addition, the energy-dispersive X-ray spectroscopy (EDS) was used to analyze the chemical composition of 3D interconnected Bi₂S₃ nanosheets (Fig. 4j), in which the signals of C and Cu can be attributed to the carbon-based copper grid. The elements of Bi and S were also detected, and the atomic ratio of Bi/S is about 2:3, which is in accordance with the stoichiometric ratio of Bi₂S₃.

3.2. Measurements of electrochemical performance

3.2.1. Electrochemical properties of the pristine Bi₂S₃, Bi₂S₃/Ni foam and AC in a three-electrode system

To investigate the electrochemical performances of the pristine Bi₂S₃, Bi₂S₃/Ni foam and AC as electrode materials in supercapacitors, CV, GCD and EIS tests were performed using a half cell in a three-electrode system. Fig. 5a–b exhibit the CV curves of the pristine Bi₂S₃ and Bi₂S₃/Ni foam in 1 M KOH aqueous electrolyte at different scan rates in the potential ranging from −0.2 to 0.6 V. The CV curves in Fig. 5a–b show some well-defined redox peaks at about 0.3 and 0.5 V, which are in good accordance with Pandit's results [45]. The non-rectangular shapes indicate the battery-type behaviors of the synthesized electrodes and the redox reaction is mainly induced by the possible reversible conversion [38,45]:



Moreover, the redox peaks shift to more positive or negative under the incremental scan rates, which may be ascribed to the increase of the internal diffusion resistances in the two electrodes [46]. In addition, at a scan rate of 10 mV s^{−1}, the CV curve integral area of the Bi₂S₃/Ni foam is larger than that for the pristine Bi₂S₃, indicating the better capacity value of the former electrode material (Fig. 5c). Fig. 5d–e show the GCD curves of the pristine Bi₂S₃ and Bi₂S₃/Ni foam at a potential range from −0.2 to 0.6 V under different current densities, and the specific capacities of the pristine Bi₂S₃ and Bi₂S₃/Ni foam are calculated from the GCD tests using Eq. (1) and are shown in Fig. 5f [37]. The specific capacity values of Bi₂S₃/Ni foam are 500.8, 440, 434.4, 428, 411 and 400 mAh g^{−1} at 0.5, 1, 1.5, 2, 3 and 4 A g^{−1}, which are higher than those (245.5, 197, 183, 150, 132 and 80 mAh g^{−1}) of the pristine Bi₂S₃ at the same current densities, and even higher than those reported in literatures (Table 1, Q was calculated according to Eq. (2)). The high capacity of Bi₂S₃/Ni foam may be attributed to its special structure (3D interconnected network), which can offer more chemical reaction sites

and afford faster ion and electron transfer in charge/discharge processes. Fig. 5g shows the Nyquist plots of the pristine Bi₂S₃ and Bi₂S₃/Ni foam. Obviously, compared with the pristine Bi₂S₃, Bi₂S₃/Ni foam possesses smaller charge transfer resistance (the radius in the high frequency region) and Warburg resistance (phase angle).

Fig. 6a–b show the CV and GCD curves of AC. The shape of the CV curves is almost rectangular, indicating the charge storage mechanism of electrochemical double layers for AC [47]. The specific capacitance of AC is calculated using Eq. (3), and the values are respectively 115.6 and 90.8 F g^{−1} at 0.5 and 1 A g^{−1}. The Nyquist plots for AC in Fig. 6c shows that it possesses low Warburg resistance and charge transfer resistance.

3.2.2. Hybrid asymmetric supercapacitor based on Bi₂S₃/Ni foam and AC

The Bi₂S₃/Ni foam//AC hybrid asymmetric supercapacitor was assembled combining Bi₂S₃/Ni foam with battery-type oxidation-reduction reaction and AC with electrochemical double layers mechanism. The mass loadings of Bi₂S₃/Ni foam (positive electrode) and AC (negative electrode) are about 3 mg respectively. Fig. 7a–c show the schematic illustration, CV and GCD curves of the Bi₂S₃/Ni foam//AC hybrid asymmetric device. The GCD curves of the Bi₂S₃/Ni foam//AC hybrid asymmetric supercapacitor in Fig. 7c are almost symmetric, indicating its reversible charge-discharge capability. The specific capacitances of the hybrid asymmetric supercapacitor were calculated using Eq. (4) from GCD curves. As shown in Fig. 7d, the specific capacitances for this hybrid asymmetric supercapacitor are respectively 148.7, 143.6, 140.1, 135.6, 131.2 and 126.8 F g^{−1} at 1, 1.5, 2, 2.5, 3 and 4 A g^{−1}. Compared with the reported specific capacitance (61 F g^{−1} at 0.25 A g^{−1}) for CoS carbonate hydroxides/Ni foam/graphene [53], the Bi₂S₃/Ni foam//AC hybrid asymmetric supercapacitor possesses higher specific capacitance.

Fig. 7e shows the Ragone plot (energy density/power density) for the Bi₂S₃/Ni foam//AC hybrid asymmetric supercapacitor. Energy density and power density were calculated according to Eq. (5) and Eq. (6). The energy densities are 52.8 Wh Kg^{−1} at 800.8 W Kg^{−1}, 51.1 Wh Kg^{−1} at 1202.5 W Kg^{−1}, 49.8 Wh Kg^{−1} at 1599.7 W Kg^{−1}, 48.2 Wh Kg^{−1} at 1999.8 W Kg^{−1}, 46.7 Wh Kg^{−1} at 2399.7 W Kg^{−1} and 45.1 Wh Kg^{−1} at 3202.8 W Kg^{−1}, which are higher than those reported in literatures (Table 2). Cycling life of the Bi₂S₃/Ni foam//AC hybrid asymmetric supercapacitor was measured by GCD cycles between 0 and 1.6 V at a scan rate of 3 A g^{−1} (Fig. 7f, the inset in Fig. 7f shows the first and last ten cycles). This device can retain about 98.7% of the initial capacitance after 2000 cycles. The capacitance retention is higher than that for the reported device, e.g. PEDOP/Bi₂S₃//Gr cell (96% after 1000 cycles) [9]. The excellent stability may be attributed to the 3D interconnected network of Bi₂S₃ and the good conductivity of AC.

Fig. 7g shows the Nyquist plot of the Bi₂S₃/Ni foam//AC hybrid asymmetric supercapacitor. The device possesses low charge transfer resistance (the radius in the high frequency region) and Warburg resistance (straight line in low frequency region), which results in fast ions transfer rate.

4. Conclusions

In summary, “rock-candy” shape Bi₂S₃ nanocrystals and 3D interconnected Bi₂S₃ nanosheets network on Ni foam were successfully synthesized by a facile hydrothermal approach. The Bi₂S₃/Ni foam was directly utilized as a binder-free working electrode. The specific capacities of “rock-candy” shape Bi₂S₃ nanocrystals in a three-electrode system are respectively 245.5, 197, 183, 150, 132 and 80 mAh g^{−1} at 0.5, 1, 1.5, 2, 3 and 4 A g^{−1}. Compared with the pristine Bi₂S₃, the Bi₂S₃/Ni foam possesses higher capacities and the values are 500.8, 440, 434.4, 428, 411 and 400 mAh g^{−1} respectively at the same current densities. In order to evaluate the actual application of Bi₂S₃/Ni foam, the Bi₂S₃/Ni foam//AC hybrid asymmetric supercapacitor was constructed by combining Bi₂S₃/Ni foam with battery-type oxidation-

reduction reaction and AC with electrochemical double layers mechanism. The hybrid asymmetric device exhibited excellent supercapacitive performances: high specific capacitance (148.7 F g^{-1} at 1 A g^{-1}); high energy density (45.1 Wh Kg^{-1} at 3202.8 W Kg^{-1}); excellent cycling stability (capacitance retention is about 98.7% after 2000 cycles at a current density of 3 A g^{-1}); low Warburg resistance and charge transfer resistance. Hence, $\text{Bi}_2\text{S}_3/\text{Ni}$ foam is a promising supercapacitor electrode material due to its excellent supercapacitive performances.

Acknowledgements

This work was supported by the National Science Foundation of China (51573126).

References

- [1] S.G. Mohamed, C.J. Chen, C.K. Chen, S.F. Hu, R.S. Liu, High-performance lithium-ion battery and symmetric supercapacitors based on FeCo_2O_4 nanoflakes electrodes, *ACS Appl. Mater. Interfaces* 6 (2014) 22701–22708.
- [2] X.Y. Zhou, G.H. Chen, J.J. Tang, Y.P. Ren, J. Yang, One-dimensional NiCo_2O_4 nanowire arrays grown on nickel foam for high-performance lithium-ion batteries, *J. Power Sources* 299 (2015) 97–103.
- [3] B.G. Zhu, S.C. Tang, S. Vongehr, H. Xie, X.K. Meng, Hierarchically MnO_2 -nanosheet covered submicrometer- FeCo_2O_4 -tube forest as binder-free electrodes for high energy density all-solid-state supercapacitors, *ACS Appl. Mater. Interfaces* 8 (2016) 4762–4770.
- [4] X.Y. Xu, Y.H. Song, R.N. Xue, J.K. Zhou, J.P. Gao, F.B. Xing, Amorphous CoMoS_4 for a valuable energy storage material candidate, *Chem. Eng. J.* 301 (2016) 266–275.
- [5] H. Wang, Y.H. Song, J.K. Zhou, X.Y. Xu, W. Hong, J. Yan, R.N. Xue, H.L. Zhao, Y. Liu, J.P. Gao, High-performance supercapacitor materials based on polypyrrole composites embedded with core-sheath polypyrrole/ MnM_2O_4 nanorods, *Electrochim. Acta* 212 (2016) 775–783.
- [6] G.D. Nie, X.F. Lu, J.Y. Lei, L. Yang, C. Wang, Facile and controlled synthesis of bismuth sulfide nanorods-reduced graphene oxide composites with enhanced supercapacitor performance, *Electrochim. Acta* 154 (2015) 24–30.
- [7] C. Wu, J.J. Cai, Q.B. Zhang, X. Zhou, Y. Zhu, L.J. Li, P.K. Shen, K.L. Zhang, Direct growth of urchin-like ZnCo_2O_4 microspheres assembled from nanowires on nickel foam as high-performance electrodes for supercapacitors, *Electrochim. Acta* 169 (2015) 202–209.
- [8] X.Y. Xu, H.L. Zhao, J.K. Zhou, R.N. Xue, J.P. Gao, NiCo_2O_4 flowers grown on the aligned-flakes coated Ni foam for application in hybrid energy storage, *J. Power Sources* 329 (2016) 238–246.
- [9] R. Mukkabl, M. Deepa, A.K. Srivastava, Poly(3,4-ethylenedioxythiophene) enwrapped Bi_2S_3 Nanoflowers for rigid and flexible supercapacitors, *Electrochim. Acta* 164 (2015) 171–181.
- [10] X.W. Xu, J.F. Shen, N. Li, M.X. Ye, Facile synthesis of reduced graphene oxide/ CoWO_4 nanocomposites with enhanced electrochemical performances for supercapacitors, *Electrochim. Acta* 150 (2014) 23–34.
- [11] R.W. Zhu, S. Murali, M.D. Stoller, K.J. Ganesh, W.W. Cai, P.J. Ferreira, A. Pirkle, Y.M. Wallace, K.A. Cychosz, M. Thommes, D. Su, E.A. Stach, R.S. Ruoff, Carbon-based supercapacitors produced by activation of graphene, *Science* 332 (2011) 1537–1541.
- [12] G.J. He, J.M. Li, W.Y. Li, B. Li, N. Noor, K.B. Xu, J.Q. Hu, I.P. Parkin, One pot synthesis of nickel foam supported self-assembly of NiWO_4 and CoWO_4 nanostructures that act as high performance electrochemical capacitor electrodes, *J. Mater. Chem.* 3 (2015) 14272–14278.
- [13] X. Chun, M. Chang, A self-assembled hierarchical nanostructure comprising carbon spheres and graphene nanosheets for enhanced supercapacitor performance, *Energy Environ. Sci.* 4 (2011) 4504–4507.
- [14] D.N. Futaba, K. Hata, T. Yamada, T. Hiraoka, Y. Hayamizu, Y. Kakudate, O. Tanaike, H. Hatori, M. Yumura, S. Iijima, Shape-engineerable and highly densely packed single-walled carbon nanotubes and their application as supercapacitor electrodes, *Nat. Mater.* 5 (2006) 987–994.
- [15] B.C. Kim, J.M. Ko, G.G. Wallace, A novel capacitor material based on Nafion-doped polypyrrole, *J. Power Sources* 177 (2008) 665–668.
- [16] S.W. Woo, K. Dokk, K. Kanamura, Composite electrode composed of bimodal porous carbon and polypyrrole for electrochemical capacitors, *J. Power Sources* 185 (2008) 1589–1593.
- [17] B. De, J. Balamurugan, N.H. Kim, J.H. Lee, Enhanced electrochemical and photocatalytic performance of core-shell $\text{CuS}@$ carbon quantum dots/ $\text{carbon hollow nanospheres}$, *ACS Appl. Mater. Interfaces* 9 (2017) 2459–2468.
- [18] X.X. Zang, Z.Y. Dai, J. Yang, Y.Z. Zhang, W. Huang, X.C. Dong, Template-assisted synthesis of nickel sulfide nanowires: tuning the compositions for supercapacitors with improved electrochemical stability, *ACS Appl. Mater. Interfaces* 8 (2016) 24645–24651.
- [19] X.F. Li, J.F. Shen, N. Li, M.X. Ye, Fabrication of γ - MnS/rGO composite by facile one-pot solvothermal approach for supercapacitor applications, *J. Power Sources* 282 (2015) 194–201.
- [20] S.G. Liu, C.P. Mao, Y.B. Niu, F.L. Yi, J.K. Hou, S.Y. Lu, J. Jiang, M.W. Xu, C.M. Li, Facile synthesis of novel networked ultralong cobalt sulfide nanotubes and its application in supercapacitors, *ACS Appl. Mater. Interfaces* 7 (2015) 25568–25573.
- [21] H.Y. Quan, B.C. Cheng, D.Z. Chen, X.H. Su, Y.H. Xiao, S.J. Lei, One-pot synthesis of α - MnS /nitrogen-doped reduced graphene oxide hybrid for high-performance asymmetric supercapacitors, *Electrochim. Acta* 210 (2016) 557–566.
- [22] F.L. Luo, J. Li, H.Y. Yuan, D. Xiao, Rapid synthesis of three-dimensional flower-like cobalt sulfide architectures by microwave assisted heating method for high-performance supercapacitors, *Electrochim. Acta* 123 (2014) 183–189.
- [23] Y.F. Tang, T. Chen, S.X. Yu, Y.Q. Qiao, S.C. Mu, S.H. Zhang, Y.F. Zhao, L. Hou, W.W. Huang, F.M. Gao, A highly electronic conductive cobalt nickel sulphide dendrite/quasispherical nanocomposite for a supercapacitor electrode with ultra-high areal specific capacity, *J. Power Sources* 295 (2015) 314–322.
- [24] H. Chauhan, M.K. Singh, P. Kumar, S.A. Hashmi, S. Deka, Development of SnS_2/RGO nanosheet composite for cost-effective aqueous hybrid supercapacitors, *Nanotechnology* 28 (2017) 025401.
- [25] Y. Ma, Y.L. Jia, L.N. Wang, M. Yang, Y.P. Bi, Y.X. Qi, One-pot synthesis of hierarchical Bi_2S_3 - MoS_2 nanosheet array with high electrochemical performance, *J. Power Sources* 342 (2017) 921–928.
- [26] S.S. Warule, N.S. Chaudhari, B.B. Kale, S. Pandiraj, R.T. Khare, M.A. More, Controlled synthesis of aligned Bi_2S_3 nanowires, sharp apex nanowires and nanobelts with its morphology dependent field emission investigations, *CrystEngComm* 15 (2013) 890.
- [27] G. Li, X.S. Chen, G.D. Gao, Bi_2S_3 microspheres grown on graphene sheets as low-cost counter-electrode materials for dye-sensitized solar cells, *Nanoscale* 6 (2014) 3283.
- [28] G. Konstantatos, L. Levina, J. Tang, E.H. Sargent, Sensitive solution-processed Bi_2S_3 nanocrystalline photodetectors, *Nano Lett* 8 (2008) 4002–4006.
- [29] J.F. Ni, Y. Zhao, T.T. Liu, H.H. Zheng, L.J. Gao, C.L. Yan, L. Li, Strongly coupled Bi_2S_3 /CNT hybrids for robust lithium storage, *Adv. Energy Mater.* 4 (2014) 1400798.
- [30] S.R. Luo, F. Chai, L.Y. Zhang, C.G. Wang, L. Li, X.C. Liu, Z.M. Su, Facile and fast synthesis of urchin-shaped Fe_3O_4 / Bi_2S_3 core-shell hierarchical structures and their magnetically recyclable photocatalytic activity, *J. Mater. Chem.* 22 (2012) 4832–4836.
- [31] Y. Zhang, J. Xu, Y.Y. Zheng, X.Y. Hu, Y.Y. Shang, Y.J. Zhang, Interconnected CuS nanowalls with rough surfaces grown on nickel foam as high-performance electrodes for supercapacitors, *RSC Adv.* 6 (2016) 59976–59983.
- [32] J.H. Shi, X.C. Li, G.H. He, L. Zhang, M. Li, Electrodeposition of high-capacity 3D CoS /graphene nanosheets on nickel foam for high-performance aqueous asymmetric supercapacitors, *J. Mater. Chem.* 3 (2015) 20619–20626.
- [33] D.K. Nandi, S. Sahoo, S. Sinha, S. Yeo, H. Kim, R.N. Bulakhe, J. Heo, J.J. Shim, S.H. Kim, Highly uniform atomic layer-deposited MoS_2 /3D-Ni-foam: anovel approach to prepare an electrode for supercapacitors, *ACS Appl. Mater. Interfaces* 9 (2017) 40252–40264.
- [34] Y.L. Xu, W.M. Du, L.L. Du, W.J. Zhu, W. Guo, J.J. Chang, B. Zhang, D.H. Deng, Monocrystalline NiS nanowire arrays supported by Ni foam as binder-free electrodes with outstanding performances, *RSC Adv.* 7 (2017) 22553–22557.
- [35] V.S. Kumbhar, Y.R. Lee, C.S. Ra, D. Tuma, B.K. Mind, J.J. Shim, Modified chemical synthesis of MnS nanoclusters on nickel foam for high performance all-solid-state asymmetric supercapacitors, *RSC Adv.* 7 (2017) 16348–16359.
- [36] J.H. Wu, C.B. Ouyang, S. Dou, S.Y. Wang, Hybrid NiS/CoO mesoporous nanosheet arrays on Ni foam for high-ratesupercapacitors, *Nanotechnology* 26 (2015) 325401.
- [37] I. Aldama, V. Barranco, T.A. Centeno, J. Ibanez, J.M. Rojo, Composite electrodes made from carbon cloth as supercapacitor material and manganese and cobalt oxide as battery one, *J. Electrochem. Soc.* 163 (2016) A758–A765.
- [38] T. Brousse, D. Belanger, J.W. Long, To be or not to be pseudocapacitive? *J. Electrochem. Soc.* 162 (2015) A5185–A5189.
- [39] H. Pang, Y.Z. Zhang, Z. Run, W.Y. Lai, W. Huang, Lamellar $\text{K}_2\text{Co}_3(\text{P}_2\text{O}_7)_2 \cdot 2\text{H}_2\text{O}$ nanocrystal whiskers: high-performance flexible all-solid-state asymmetric micro-supercapacitors via inkjet printing, *Nanomater. Energy* 15 (2015) 303–312.
- [40] W.H. Shin, H.M. Jeong, B.G. Kim, J.K. Kang, J.W. Choi, Nitrogen-doped multiwall carbon nanotubes for lithium storage with extremely high capacity, *Nano Lett.* 12 (2012) 2283–2288.
- [41] Y. Zheng, T.F. Zhou, X.D. Zhao, W.K. Pang, H. Gao, S. Li, Z. Zhou, H.K. Liu, Z.P. Guo, Atomic interface engineering and electric-field effect in ultrathin Bi_2MoO_6 nanosheets for superior lithium ion storage, *Adv. Mater.* 29 (2017) 1700396.
- [42] X.M. Gao, G.B. Huang, H.H. Gao, C. Pan, H. Wang, J. Yan, Y. Liu, H.X. Qiu, N. Ma, J.P. Gao, Facile fabrication of $\text{Bi}_2\text{S}_3/\text{SnS}_2$ heterojunction photocatalysts with efficient photocatalytic activity under visible light, *J. Alloy. Comp.* 674 (2016) 98–108.
- [43] B. Zhang, X.C. Ye, W.Y. Hou, Y. Zhao, Y. Xie, Biomolecule-assisted synthesis and electrochemical hydrogen storage of Bi_2S_3 flower like patterns with well-aligned nanorods, *J. Phys. Chem. B* 110 (2006) 8978–8985.
- [44] L.S. Li, N.J. Sun, Y.Y. Huang, Y. Qin, N.N. Zhao, J.N. Gao, M.X. Li, H.H. Zhou, L.M. Qi, Topotactic transformation of single-crystalline precursor discs into disc-like Bi_2S_3 nanorod networks, *Adv. Funct. Mater.* 18 (2008) 1194–1201.
- [45] B. Pandit, G.K. Sharma, B.R. Sankpal, Chemically deposited $\text{Bi}_2\text{S}_3/\text{PbS}$ solid solution thin film as supercapacitive electrode, *J. Colloid Interface Sci.* 505 (2017) 1011–1017.
- [46] J. Yan, Z. Fan, W. Sun, G. Ning, T. Wei, Q. Zhang, R. Zhang, L. Zhi, F. Wei, Advanced asymmetric supercapacitors based on $\text{Ni}(\text{OH})_2/\text{graphene}$ and porous graphene electrodes with high energy density, *Adv. Funct. Mater.* 22 (2012) 2632–2641.
- [47] Y.M. Wang, J.C. Chen, J.Y. Cao, Y. Liu, Y. Zhou, J.H. Ouyang, D.C. Jia, Graphene/carbon black hybrid film for flexible and high rate performance supercapacitor, *J. Power Sources* 271 (2014) 269.
- [48] H.C. Lu, Q.B. Guo, F. Zan, H. Xia, Bi_2S_3 nanoparticles anchored on graphene

- nanosheets with superior electrochemical performance for supercapacitors, *Mater. Res. Bull.* 96 (2017) 471–477.
- [49] S. Ratha, C.S. Rout, Supercapacitor electrodes based on layered tungsten disulfide reduced graphene oxide hybrids synthesized by a facile hydrothermal method, *ACS Appl. Mater. Interfaces* 5 (2013) 11427–11433.
- [50] H.Z. Wan, X. Ji, J.J. Jiang, J.W. Yu, L. Miao, L. Zhang, S.W. Bie, H.C. Chen, Y.J. Ruan, Hydrothermal synthesis of cobalt sulfide nanotubes: the size control and its application in supercapacitors, *J. Power Sources* 243 (2013) 396–402.
- [51] S. Vadivel, A.N. Naveen, V.P. Kamalakannan, P. Cao, N. Balasubramanian, Facile large scale synthesis of Bi_2S_3 nanorods–graphene composite for photocatalytic photoelectrochemical and supercapacitor application, *Appl. Surf. Sci.* 351 (2015) 635–645.
- [52] M.Q. Wang, H.F. Fei, P. Zhang, L.W. Yin, Hierarchically layered $\text{MoS}_2/\text{Mn}_3\text{O}_4$ hybrid architectures for electrochemical supercapacitors with enhanced performance, *Electrochim. Acta* 209 (2016) 389–398.
- [53] S. Liu, K.S. Hui, K.N. Hui, V.V. Jadhav, Q.X. Xia, J.M. Yun, Y.R. Cho, R.S. Mane, K.H. Kim, Facile synthesis of microsphere copper cobalt carbonate hydroxides electrode for asymmetric supercapacitor, *Electrochim. Acta* 188 (2016) 898.
- [54] C.J. Raj, B.C. Kim, W.J. Cho, W.G. Lee, Y. Seo, K.H. Yu, Electrochemical capacitor behavior of copper sulfide (CuS) nanoplatelets, *J. Alloy. Comp.* 586 (2014) 191–196.